Second-Order Discretization in Space and Time for Radiation-Hydrodynamics

Simon Bolding[a], Joshua Hansel[a], Jarrod D. Edwards[b], Jim E. Morel[a], Robert B. Lowrie[c]

[a]*Department of Nuclear Engineering, 337 Zachry Engineering Center, TAMU 3133, Texas A&M University, College Station, Texas, 77843*
[b]*Phenomenology and Sensor Science Department, Sandia National Laboratory, Albuquerque, NM*
[c]*Computational Physics Group CCS-2, Los Alamos National Laboratory, P.O. Box 1663, MS D413, Los Alamos, NM 87545*

Abstract

Second-order accurate discretizations for radiation-hydrodynamics are currently an area of great interest. Second-order methods used to solve the hydrodynamics equations and second-order methods used to solve the radiation transport equation often differ fundamentally, making it difficult to combine them in a second-order manner. Here, we present a implicit-explicit (IMEX) method for solving the 1-D equations of radiation-hydrodynamics that is second-order accurate in space and time. Our radiation-hydrodynamics model consist of the 1-D Euler equations coupled with a grey radiation S_2 approximation. Our RH method combines the MUSCL-Hancock method for solving the Euler equations with the TR/BDF2 time integration scheme and the linear-discontinuous Galerkin finite-element spatial discretization scheme for the S_2 radiation equations. The MUSCL-Hancock method is commonly used for hydrodynamic calculations and the linear-discontinuous Galerkin scheme is the standard for the S_n equations of radiative transfer. While somewhat similar, these schemes vary fundamentally with respect to the treatment of spatial slopes. We address the challenges inherent to coupling these different numerical methods and demonstrate how these challenges can be overcome. Using the method of manufactured solutions, we show that the method is second-order accurate in space and time for both the equilibrium diffusion and streaming limit, and we show that the method is capable of computing radiative shock solutions accurately by comparing our results with semi-analytic solutions.

Preprint submitted to Journal of Computational Physics *May 16, 2016*

Keywords: radiation-hydrodynamics, second-order accuracy, radiative shocks, manufactured solutions, MUSCL Hancock, TR/BDF2

1. Introduction

Radiation hydrodynamics (RH) describes thermal radiation propagating through a fluid and the effects of the radiation on the properties of that fluid. Second-order accuracy in time for radiation-hydrodynamics calculations is currently an area of considerable interest. Though detailed work has been done for time integration of radiation diffusion and transport [1, 2, 3, 4, 5, 6, 7], and likewise for fluid dynamics [8], research in second-order methods that couple the two has only recently been carried out [9, 10, 11]. Because of the dramatically different time scales of radiation diffusion/transport and fluid advection, RH calculations are usually treated using an implicit-explicit (IMEX) scheme [9, 10, 11]. In such algorithms, the fluid advection component, which changes at a much slower rate, is treated explicitly; whereas, the radiation diffusion and radiation energy exchange terms are treated implicitly.

Sekora and Stone developed a scheme for RH that uses second-order Godunov methods to achieve second-order accuracy in space and time. This scheme is entirely explicit so that the time step is limited by the more rapidly varying radiation time scale [12]. Sekora's method is intended for the relativistic regime characterized as $a_\infty/c < 0.1$, where a_∞ denotes the speed of sound of the material and c denotes the speed of light. In this case, the fluid and radiation time-scales are not dramatically different, and therefore, the Courant limit time-step constraint is not overly restrictive. However, for the non-relativistic regime, i.e. $a_\infty/c < .01$, bounding the time-step according to the radiation time-scale will force the time steps to be at least two orders of magnitude smaller than the fluid time-scale. Kadioglu has also developed a second-order accurate scheme for both low and high energy density RH problems [13, 14]. Accuracy is achieved by incorporating the explicit algorithm into the implicit iterations. While this provides a tight coupling between the explicit and implicit terms, it is computationally more expensive than standard IMEX schemes, since the explicit block is solved in each nonlinear iteration [13].

In this work, we derive, implement, and test a new IMEX scheme for solving the equations of radiation hydrodynamics that is second-order accurate

in both space and time. We consider a 1-D RH system that combines a 1-D slab model of compressible fluid dynamics with a grey radiation S_2 model, given by:

$$\frac{\partial \rho}{\partial t} + \frac{\partial}{\partial x}(\rho u) = 0\,, \tag{1a}$$

$$\frac{\partial}{\partial t}(\rho u) + \frac{\partial}{\partial x}\left(\rho u^2\right) + \frac{\partial}{\partial x}(p) = \frac{\sigma_t}{c} F_{r,0}\,, \tag{1b}$$

$$\frac{\partial E}{\partial t} + \frac{\partial}{\partial x}\left[(E+p)\,u\right] = -\sigma_a c\left(aT^4 - E_r\right) + \frac{\sigma_t u}{c} F_{r,0}\,, \tag{1c}$$

$$\frac{1}{c}\frac{\partial \psi^+}{\partial t} + \frac{1}{\sqrt{3}}\frac{\partial \psi^+}{\partial x} + \sigma_t \psi^+ = \frac{\sigma_s}{4\pi} c E_r + \frac{\sigma_a}{4\pi} acT^4 - \frac{\sigma_t u}{4\pi c} F_{r,0} + \frac{\sigma_t}{\sqrt{3}\pi} Eu\,, \tag{1d}$$

$$\frac{1}{c}\frac{\partial \psi^-}{\partial t} - \frac{1}{\sqrt{3}}\frac{\partial \psi^-}{\partial x} + \sigma_t \psi^- = \frac{\sigma_s}{4\pi} c E_r + \frac{\sigma_a}{4\pi} acT^4 - \frac{\sigma_t u}{4\pi c} F_{r,0} - \frac{\sigma_t}{\sqrt{3}\pi} Eu\,, \tag{1e}$$

where ρ is the density, u is the velocity, $E = \frac{\rho u^2}{2} + \rho e$ is the total fluid energy density, e is the specific internal energy density, T is the fluid temperature, E_r is the radiation energy density,

$$E_r = \frac{2\pi}{c}\left(\psi^+ + \psi^-\right)\,, \tag{2}$$

F_r is the radiation energy flux,

$$F_r = \frac{2\pi}{\sqrt{3}}\left(\psi^+ - \psi^-\right) \tag{3}$$

and $F_{r,0}$ is an approximation to the comoving-frame flux,

$$F_{r,0} = F_r - \frac{4}{3} E_r u\,. \tag{4}$$

Note that if we multiply Eqs. ((1d)) and (1e) by 2π and sum them, we obtain the radiation energy equation:

$$\frac{\partial E_r}{\partial t} + \frac{\partial F_r}{\partial x} = \sigma_a c(aT^4 - E_r) - \frac{\sigma_t u}{c} F_{r,0}\,, \tag{5a}$$

and if we multiply Eq. (1d) by $\frac{2\pi}{c\sqrt{3}}$, multiply Eq. (1e) by $-\frac{2\pi}{c\sqrt{3}}$ and sum them, we get the radiation momentum equation:

$$\frac{1}{c^2}\frac{\partial F_r}{\partial t} + \frac{1}{3}\frac{\partial E_r}{\partial x} = -\frac{\sigma_t}{c} F_{r,0}\,. \tag{5b}$$

Note that Eqs. (5a) and (5b) are known as the P_1 radiation approximation and are completely equivalent to Eqs. (1d) and (1e) under a similarity transformation defined by the invertible mapping given by Eqs. (2) and (3).

Equations (1a) through (1e) are closed in our calculations by assuming an ideal equation of state (EOS):

$$p = \rho e(\gamma - 1)\,, \tag{6a}$$

$$T = \frac{e}{C_v}\,, \tag{6b}$$

where γ is the adiabatic index, and C_v is the specific heat. However, our method is compatible with any valid EOS.

Our RH method combines the MUSCL-Hancock method (MHM) for solving the Euler equations with the TR/BDF2 time discretization scheme and the linear-discontinuous Galerkin finite-element (LDGFEM) spatial discretization scheme for the S_2 equations. The MUSCL-Hancock method is commonly used for hydrodynamic calculations and the linear-discontinuous Galerkin scheme is the standard for the S_n radiation equations. While somewhat similar, these schemes vary fundamentally with respect to the treatment of spatial slopes. The resolution of conflicts arising from these disparate slope treatments is a major component of our new RH method.

One of the most common methods for discretizing the S_n equations in time is the Crank-Nicholson method, also known as the Trapezoid Rule. This is a well-known, implicit method that is second-order accurate; however, its principal drawback is that it can become highly oscillatory for stiff systems. An alternative to this is a linear-discontinuous Galerkin method in time. Despite the fact that this scheme is more accurate than the Crank-Nicholson method and damps oscillations quickly, it has a much higher computational cost that is roughly equivalent to that of solving two Crank-Nicholson systems simultaneously over each time step. In this work, we use the TR/BDF2 scheme for discretizing the radiation S_2 and energy exchange terms in time. The TR/BDF2 scheme is a one-step, two-stage[1] implicit method that was first derived in [15]. There is actually a family of such schemes, but one member of the family can be shown to be optimal in a certain sense. A simple version of this method that is near-optimal was applied to the equations of radiative

[1]Here we use the term "stage" to refer to an implicit equation that must be solved within each time step in a discretization scheme.

transfer in [16], where it is shown to be both L-stable, accurate, and efficient. In [16], the near-optimal TR/BDF2 scheme is used to solve the equations of radiative transfer. It consists of a Crank-Nicholson step over half the time step and, using that solution, a BDF2 step over the remainder of the time step. The TR/BDF2 method has a computational cost that is roughly equivalent to that of solving two Crank-Nicholson systems sequentially over each time step. Here we introduce an alternative form of of the simple TR/BDF2 method that is particularly useful for our purposes.

A critical issue for radiation transport spatial discretizations is the preservation of the diffusion limit. Radiation-hydrodynamics problems often contain highly diffusive regions. In any type of calculation it is generally expected that accurate solutions will be obtained whenever the spatial variation of the solution is well-resolved by the mesh. However, use of a consistent transport discretization scheme in a highly diffusive problem will not guarantee such behavior. To ensure it, a consistent discretization scheme must "preserve" the diffusion limit or "be asymptotic preserving" [17]. A consistent discretization that does not preserve the diffusion limit will only yield accurate results in highly diffusive problems if the spatial cells are small with respect to a mean-free-path. Since the diffusion length can a arbitarily large with respect to a mean-free-path, discretization schemes that are not asymptotic preserving can be prohibitively expensive to use in problems with highly diffusive regions due to the need to arbitrarily over-resolve the solution. Thus preservation of the radiation diffusion limit is an essential property of any radiation-hydrodynamics scheme. Although we only use an S_2 radiation treatment, our overall coupling and solution scheme is applicable to an S_n treatment of arbitrary order. The only caveat is that a higher order S_n model will require a standard iterative solution technique for the S_n equations themselves rather than directly solving those equations as we do. An important aspect of our study is that we are able to investigate preservation of the diffusion limit assuming an LDFEM spatial discretization for a S_2 treatment that will be valid for an S_n treatment of arbitrary order.

The MHM includes spatial differencing for the advection equations and incorporates a linear interpolation from cell-averaged values to compute the slopes. However, Lowrie and Morel show in [18] that interpolation schemes which only depend on the mesh geometry and do not incorporate additional physical data, e.g. cross-section values, fail to have the diffusion limit. Furthermore, the differences in spatial discretization between the advection and S_2 equations present considerable complications due to the fact that, in the

MHM, the slopes are determined from interpolations of the cell-centered unknowns; whereas, in the LDFEM, the slopes are computed as part of the solution to the discretized spatial moment equations. To add to these complications, the internal energy of the fluid represents an unknown in both the fluid advection and radiation equations. The easy solution to this problem is to recompute the internal energy and radiation slopes at the beginning of each time step using the MHM limiter. Doing this, we were able to show that our method maintained the diffusion limit in 1D and reproduced shock solutions accurately. However, standard 2D and 3D hydrodynamics limiters use a spatial representation that will not maintain the radiation diffusion limit [19]. In particular, a simple linear dependence for the solution is assumed but a bilinear (2D) or a trilinear dependence (3D) is required [20]. Thus, to overcome this limitation, the method we present here retains the slopes computed by the LDFEM from one time step to the next. We use reconstructed slopes as determined in the MUSCL-Hancock method only to compute the advection fluxes, and we use the retained LDFEM slopes to initialize the implicit calculations for the radiation energy density and flux and for the fluid temperature update. This allows our method to reduce to its standard constituent methods when the contributions from coupled physics are negligible, and we believe it will also allow us to preserve the diffusion limit in a future extension of our method to 2D and 3D. Of course, this remains to be demonstrated.

The remainder of this paper is structured as follows. In Section 2, we give an overview of our second-order accurate radiation-hydrodynamics method, and we give a detailed description in the Appendix. In Section 4, we use the method of manufactured solutions to show that our method is second-order accurate in both space and time in the equilibrium diffusion limit as well as in the streaming limit. Then, in Section 5, we demonstrate the capability of our method to accurately compute radiation-hydrodynamic shocks by reproducing semi-analytic shock solutions. Finally, in Section **??**, we summarize our results and present our conclusions and recommendations for future work.

2. Overview of the Radiation-Hydrodynamics Method

There are two cycles per time step. The first cycle spans the first half of the time step and the second spans the second half. The first cycle proceeds as follows:

1. Do a standard MHM predictor step.

2. Enter an iteration loop
   (a) Update the fluid momentum using lagged radiation momentum deposition
   (b) Simultaneously solve the total energy equation and the S_2 equations for the new radiation intensities and updated fluid internal energies using an LDG discretization in space and a Crank-Nicholson discretization in time.
   (c) Continue the iteration until the fluid momenta, internal energies, and radiation intensities converge.
3. Do a standard MHM corrector step.
4. Enter an iteration loop
   (a) Update the fluid momentum using lagged radiation momentum deposition
   (b) Simultaneously solve the total energy equation and the S_2 equations for the new radiation intensities and updated fluid internal energies using an LDG discretization in space and a Crank-Nicholson discretization in time.
   (c) Continue iteration until the fluid momenta, internal energies, and radiation intensities converges.

The second cycle proceeds as follows:

1. Do a standard MHM predictor step.
2. Enter an iteration loop.
   (a) Update the fluid momentum using lagged radiation momentum deposition.
   (b) Simultaneously solve the total energy equation and the S_2 equations for the new radiation intensities and updated fluid internal energies using an LDG discretization in space and a Crank-Nicholson discretization in time.
   (c) Continue iteration until fluid momenta, internal energies, and radiation intensities converge.
3. Do a standard MHM corrector step.
4. Enter an iteration loop
   (a) Update the fluid momentum using lagged radiation momentum deposition
   (b) Simultaneously solve the total energy equation and the S_2 equations for the new radiation intensities and updated fluid internal energies using an LDG discretization in space and a BDF2 discretization in time.

(c) Continue iteration until fluid momenta, internal energies, and radiation intensities converge.

Note that the combination of Crank-Nicholson and BDF2 discretization results in a TR/BDF2 discretization over the full time step. One advantage to applying the full MHM over each half time step is that, if the time step size is being determined by the Courant limit, we can take twice the usual time step. In this case, the cost of four radiation solves per time step per iteration is mitigated. Alternatively, this algorithm could be viewed as a mixed, multistep algorithm with alternating Crank-Nicholson and BDF2 solves over time steps (from this viewpoint, the time step sizes are governed by the standard Courant limit and there is only two radiation solves per time step).

Our scheme is designed in such a way that, if the radiation contributions to the hydrodynamics are negligible, the standard MHM solution is obtained over each half time step, and if the hydrodynamics contributions to the radiation diffusion are negligible, the standard TR/BDF2 solution for radiative transfer is obtained over the full time step. The process of iterating between the radiation momentum deposition to the fluid and the nonlinear radiation/internal energy solves is necessary to conserve total momentum. The radiation momentum deposition is usually small in the high energy density laboratory physics (HEDLP) regime, so a Picard-type iteration for the momentum deposition is adequate. In problems with stronger radiation momentum deposition, a better iteration scheme might be required.

2.1. Diffusion Limit

Of importance to obtaining the diffusion limit is using the correct initial internal energy slopes in the simultaneous solve for the S_2 intensities and the updated internal energies. Each MHM step provides slopes for the mass densities, the fluid momentum densities, and the fluid total energies. From the mass and fluid momentum slopes one can compute kinetic energy slopes. These slopes are used together with the fluid internal energy slopes from the previous-cycle radiation/internal energy solve to initialize the left and right fluid total energies.

2.2. Slope limiting

McClarren and Lowrie [21] investigated the impact of slope limiting on asymptotic-preserving methods for hyperbolic systems with stiff relaxation terms that reduce to a parabolic description when relaxation dominates. This

work is relevant to our radiation-hydrodynamics method. They found that a slope limiter must not introduce discontinuities at cell edges if asymptotic preservation is to be maintained. The minmod limiter has this property and is thus not suitable for radiation-hydrodynamics in general. However, the double minmod and the "sawtooth-free" limiter introduced by Lowrie do not have this property. Here we use the double minmod limiter.

2.3. Alternate Form of TBDF2 Method

Consider a partial differential equation of the form $\frac{\partial f}{\partial t} = \mathbf{A}f(t)$. We have derived the following non-standard form of the TR/BDF2 solution method to facilitate determining the form of the radiation coupling terms in the hydrodynamics equations:

$$\frac{2\left(f^{n+1/2} - f^{n}\right)}{\Delta t} = \frac{1}{2}(\mathbf{A}f)^{n+1/2} + \frac{1}{2}(\mathbf{A}f)^{n}\,, \tag{7}$$

$$\frac{2\left(f^{n+1} - f^{n+1/2}\right)}{\Delta t} = \frac{2}{3}(\mathbf{A}f)^{n+1} + \frac{1}{6}(\mathbf{A}f)^{n+1/2} + \frac{1}{6}(\mathbf{A}f)^{n}\,. \tag{8}$$

Note that each of these expression represents a conservation statement over each half time step. The usual expression that Eq. (8) replaces is

$$\frac{3\left(f^{n+1} - f^{n+1/2}\right)}{\Delta t} - \frac{\left(f^{n+1/2} - f^{n}\right)}{\Delta t} = (\mathbf{A}f)^{n+1}\,, \tag{9}$$

which is clearly not a conservation statement. Equation (7) is used for the radiation/internal energy during the first and second cycle predictor steps and the first cycle corrector step. Equation (8) is used for the radiation/internal energy during the second cycle corrector step.

3. Results for the Method of Manufactured Solutions

4. Second-Order Accuracy

To demonstrate that our method is second-order accurate in space and time, we use the method of manufactured solutions (MMS). With MMS, we assume a functional form of the exact solution and use that to derive a set of forcing functions. These forcing functions can then be used to reproduce those solutions with our numerical method. This allows us to prescribe an exact solution with sufficient variation in space and time to fully test the

coupling between the radiation and hydrodynamics while ensuring that the solution space is smooth. By comparing our results, generated using these forcing functions, with the exact solution as we refine the solution in space and time, we can examine the behavior of the error to determine order-accuracy.

For these tests, we use the manufactured solutions developed by McClarren and Lowrie in [**?**] as a foundation. These solutions are composed of a combination of trigonometric functions with periodic boundary conditions. Our manufactured sources are a modification of those in [**?**], which uses a P_1 radiation model. As in [**?**], we consider both an equilibrium diffusion limit and a streaming limit solution.

This manufactured solution affords us the opportunity to test the behavior of our method in the equilibrium diffusion limit. To test this limit, we examine the error of the solution as the mesh is refined while preserving the optical thickness, τ, of each cell. The error of a method that preserves the equilibrium diffusion limit will decrease as the mesh is refined for a fixed τ and CFL condition; however, a method that does not have this limit will only converge to the correct solution if τ decreases with the mesh spacing. In order to test the thick diffusion limit, it is necessary to set $\tau >> 1$. For our test problems, we set $\tau = 100\pi$, $\alpha = 0.5$, $\gamma = 5/3$, and $\mathbb{P} = 0.001$. To keep τ constant as we vary the mesh spacing, we define a parameter ϵ and vary Δx, $\mathbb{C}$, and σ with ϵ as follows:

To test the full radiation-hydrodynamics system, an MMS (Method of Manufactured Solutions) problem was designed. The original system given by Equations (1a) through (1c) and (**??**) is the following:

$$\frac{\partial \rho}{\partial t} + \frac{\partial}{\partial x}\left(\rho u\right) = 0\,,$$

$$\frac{\partial}{\partial t}\left(\rho u\right) + \frac{\partial}{\partial x}\left(\rho u^2\right) + \frac{\partial}{\partial x}\left(p\right) = \frac{\sigma_t}{c}\mathcal{F}_0\,,$$

$$\frac{\partial E}{\partial t} + \frac{\partial}{\partial x}\left[\left(E+p\right)u\right] = -\sigma_a c\left(aT^4 - \mathcal{E}\right) + \frac{\sigma_t u}{c}\mathcal{F}_0\,,$$

$$\frac{1}{c}\frac{\partial \Psi^{\pm}}{\partial t} + \mu^{\pm}\frac{\partial \Psi^{\pm}}{\partial x} + \sigma_t \Psi^{\pm} = \frac{\sigma_s}{2}\phi + \mathcal{Q}^{\pm}\,.$$

To execute an MMS problem, extraneous source terms are added to the system as follows:

$$\frac{\partial \rho}{\partial t} + \frac{\partial}{\partial x}\left(\rho u\right) = Q^{ext,\rho}\,, \tag{10a}$$

$$\frac{\partial}{\partial t}(\rho u) + \frac{\partial}{\partial x}\left(\rho u^2\right) + \frac{\partial}{\partial x}(p) = \frac{\sigma_t}{c}\mathcal{F}_0 + Q^{ext,\rho u}\,, \tag{10b}$$

$$\frac{\partial E}{\partial t} + \frac{\partial}{\partial x}\left[(E+p)\,u\right] = -\sigma_a c\left(aT^4 - \mathcal{E}\right) + \frac{\sigma_t u}{c}\mathcal{F}_0 + Q^{ext,E}\,, \tag{10c}$$

$$\frac{1}{c}\frac{\partial \Psi^{\pm}}{\partial t} + \mu^{\pm}\frac{\partial \Psi^{\pm}}{\partial x} + \sigma_t \Psi^{\pm} = \frac{\sigma_s}{2}\phi + \mathcal{Q}^{\pm} + Q^{ext,\pm}\,. \tag{10d}$$

Two MMS problems, one for the streaming limit and one for the equilibrium diffusion limit, were taken from [**?**].

For the diffusion limit problem, the following solutions were prescribed for the hydrodynamic solution:

$$\rho = A\left(\sin(Bx - Ct) + 2\right)\,, \tag{11a}$$

$$u = A\left(\cos(Bx - Ct) + 2\right)\,, \tag{11b}$$

$$p = A\alpha\left(\cos(Bx - Ct) + 2\right)\,, \tag{11c}$$

where A, B, and C are constants to be chosen. As stated in [**?**], the radiation energy density and flux are the following in the equilibrium diffusion limit:

$$\mathcal{E} = T^4\,, \tag{12a}$$

$$\mathcal{F} = \frac{1}{3\sigma}\partial_x T^4 + \frac{4}{3}\frac{u}{\mathbb{C}}T^4\,, \tag{12b}$$

where $\mathbb{C}$ is a non-dimensional parameter. Using the ideal gas equation of state relations, an expression for temperature T can be derived and substituted into these equations, using a specific heat c_v such that

$$T = \frac{\gamma p}{\rho}\,. \tag{13}$$

Symbolic manipulation can be used to derive the MMS sources Q^{ρ}, $Q^{\rho u}$, Q^{E}, and $Q^{\pm}$; the resulting expressions are omitted here due to their complexity and length. The values chosen for the constants/non-dimensional parameters are $A = B = C = 1$, $\alpha = 0.5$, $\gamma = \frac{5}{3}$, and $\mathbb{C} = \sigma = 1000$. Figure 1 compares the computed hydrodynamic solutions with the exact solutions for this problem, and Figure 2 shows that 2nd-order convergence is achieved (shown here for internal energy).

The second MMS problem corresponds to the streaming limit, in which the radiation and hydrodynamics are weakly coupled due to the high radiation energy propagation speed relative to the fluid speed. For this problem, the following MMS solutions are chosen:

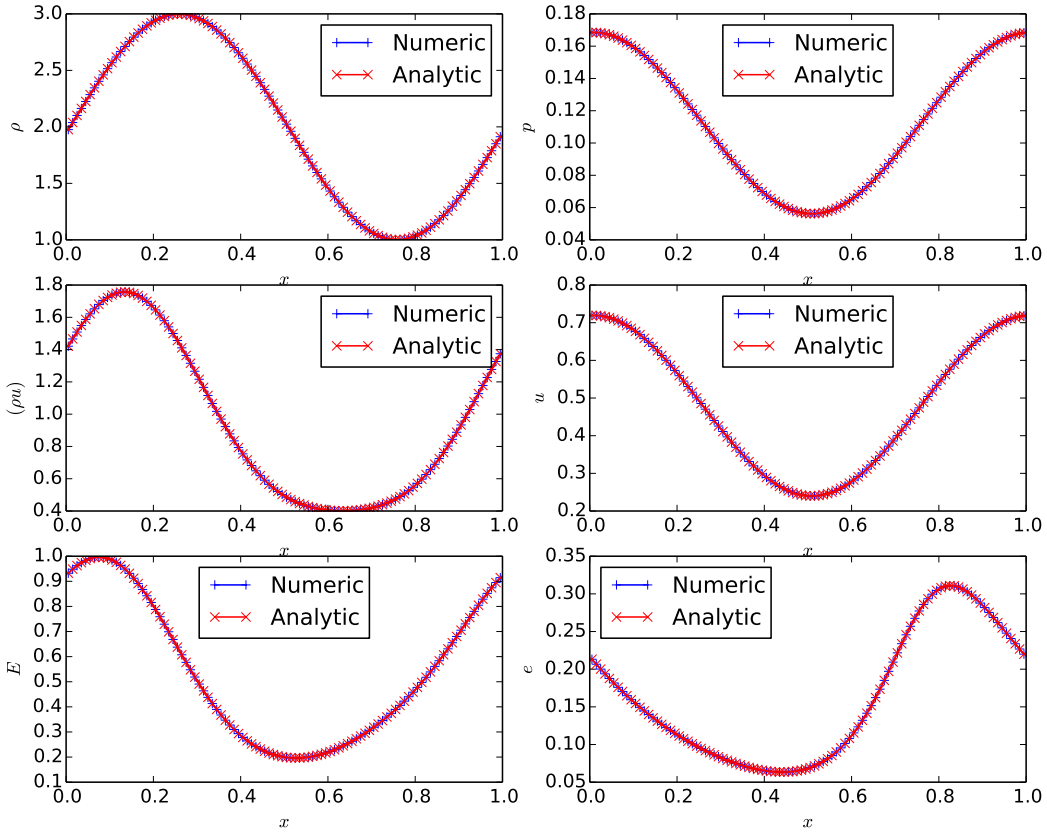

Figure 1: Hydrodynamic solution for the equilibrium diffusion limit MMS problem

4.1. Streaming Limit

Next, we consider the manufactured solution for the streaming limit. In this limit, radiation streaming dominates a relatively small radiation absorption/re-emission term. Here, we keep the re-emission term small by making the opacity relatively small so that the radiation is nearly transparent to the fluid. Therefore, in contrast to the equilibrium diffusion limit which represents very tight coupling between the radiation and hydrodynamic components, this limit represents very weak coupling between the two. Also, because the radiation streams much faster than the fluid, this results in a solution in which the unknowns evolve at significantly different time scales. The functional form of the exact streaming solution is given by:

Here, was can see that the wave speed of the radiation energy density is faster than that of the hydrodynamic unknowns by a factor of $\mathbb{C}$. This

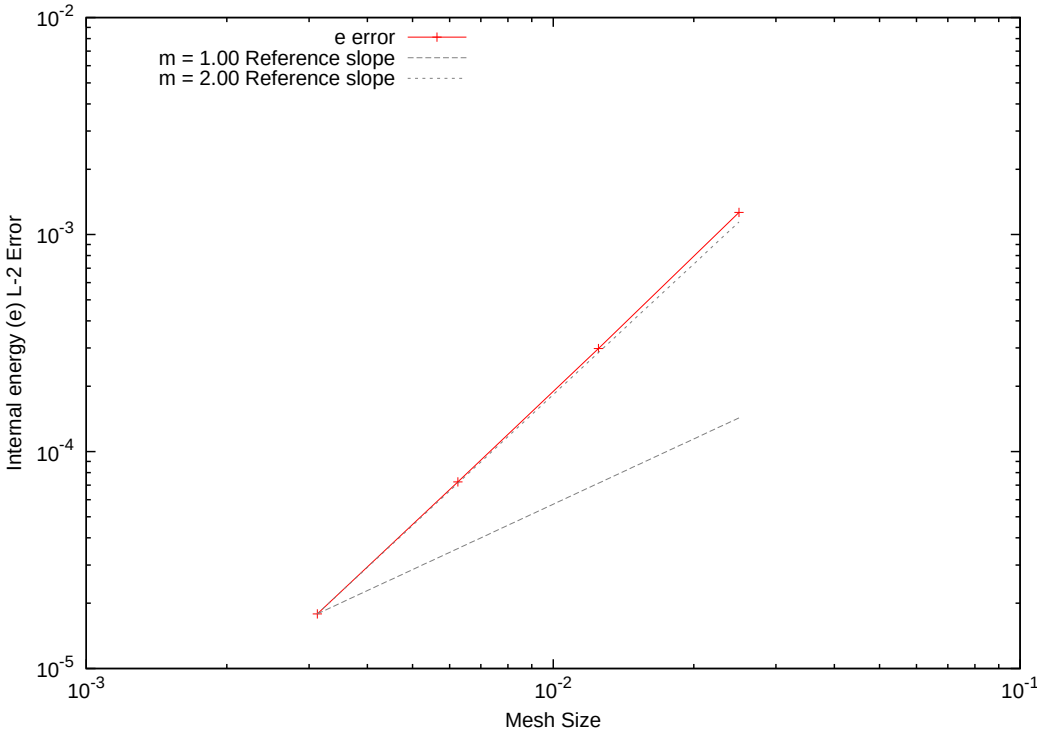

Figure 2: Convergence of internal energy for the equilibrium diffusion limit MMS problem

solution is also defined to mimic an isothermal flow regime, in which the radiation varies rapidly enough that changes in the fluid temperature are suppressed. In this case, the exact solution for the fluid temperature is a constant given by:

5. Results for Radiation-Hydrodynamic Shocks

Reproducing radiative shocks accurately, particularly in the optically thick regime, represents a challenging problem in the simulation of radiation hydrodynamics. However, because many problems of interest include radiative shocks, it is imperative that a numerical scheme be able to meet these challenges well. The widely used Zel'dovich and Raizer [**?**] and Mihalas and Mihalas [**?**] provide the classic descriptions of radiative shocks. The structure of optically thick radiative shocks, which we consider here, has been described in more detail by Drake in [**?**] and by Lowrie and Edwards in [**?**]. In the remainder of this section, we demonstrate the capability of

our rad-hydro algorithm to compute accurate radiative shock solutions by reproducing the semi-analytic shocks detailed in [**?**] and comparing our results with those of a first-order scheme.

Here, we describe our procedure to generate the shocks and compare our computational results with the semi-analytic solutions. We begin by computing the far-downstream fluid state associated with a prescribed set of far-upstream conditions. As we previously mentioned, these far-upstream conditions, and subsequently, the radiative shock itself, are specified by the shock Mach number M, the parameters $\mathbb{P}$ and σ_a, and the radiative diffusivity κ, which is given by:

$$\kappa = \frac{\hat{c}}{3\hat{\sigma}_t \hat{a}_0 \hat{L}} \,. \tag{14}$$

The equations that describe the overall jump from the upstream to the downstream states are a modified version of the Rankine-Hugoniot conditions derived by equating the flux terms from the fluid conservation equations in the rad-hydro model. These modified Rakine-Hugoniot conditions are given-by:

$$(\rho v)_0 = (\rho v)_1 \,, \tag{15a}$$

$$\left(\rho v^2 + p^*\right)_0 = \left(\rho v^2 + p^*\right)_1 \,, \tag{15b}$$

$$\left[\left(\rho E^* + p^*\right) v\right]_0 = \left[\left(\rho E^* + p^*\right) v\right]_1 \,, \tag{15c}$$

where

$$p^* = p + \frac{1}{3}\mathbb{P}T^4 \,, \tag{16a}$$

$$e^* = e + \frac{1}{\rho}\mathbb{P}T^4 \,, \tag{16b}$$

$$E^* = e^* + \frac{1}{2}v^2 \,. \tag{16c}$$

In [**?**], Lowrie and Rauenzahn show that these equations may be manipulated algebraically to solve for ρ_1:

$$\rho_1(T_1) = \frac{f_1(T_1) + \sqrt{f_1^2(T_1) + f_2(T_1)}}{6(\gamma - 1)T_1} \,, \tag{17}$$

where

$$f_1(T_1) = 3(\gamma+1)(T_1-1) - \mathbb{P}\gamma(\gamma-1)(7+T_1^4)\,, \tag{18a}$$

$$f_2(T_1) = 12(\gamma-1)^2 T_1\left[3+\gamma\mathbb{P}\left(1+7T_1^4\right)\right]\,. \tag{18b}$$

Furthermore, eliminating v_1 from the mass equation, substituting the result into the momentum equation, and rearranging terms, we have an equation for T_1:

$$3\rho_1(\rho_1 T_1 - 1) + \gamma\mathbb{P}\rho_1\left(T_1^4 - 1\right) = 3\gamma(\rho_1 - 1)M_0^2\,. \tag{19}$$

Substituting Eq. (17) into Eq. (19), this results in a ninth-order polynomial, which may be solved numerically for T_1. We initialize this solution procedure using an estimate for T_1 based on $\mathbb{P}$. For "small" values of $\mathbb{P}$, we initialize using:

$$T_1^{est} = \frac{(1-\gamma+2\gamma M^2)\left(2+(\gamma-1)M^2\right)^2}{(\gamma+1)^2 M^2}\,. \tag{20}$$

For "large" values of $\mathbb{P}$, we estimate T_1 as:

$$T_1^{est} = \sqrt[4]{\frac{8\left(\frac{M^2}{(4/9)\mathbb{P}}-1\right)}{7}}\,. \tag{21}$$

In solving for T_1, we note that the numerical solver does not always converge to the same final value for T_1 for both initial estimates. However, for the shocks considered here, in the case when the initial estimates lead to differing values of T_1, the final solution for one estimate is always non-physical. So in these cases, it is obvious which converged T_1 value is correct.

Because our radiation-hydrodynamics method is developed in dimensional form, we must also define the characteristic values $\hat{\rho}_0$ and $\hat{T}_0$. The remaining dimensionalized values are computed from the non-dimensional parameters as follows:

$$\hat{\rho}_1 = \rho_1\hat{\rho}_0\,, \tag{22a}$$

$$\hat{T}_1 = T_1\hat{T}_0\,, \tag{22b}$$

$$\hat{a_0} = \sqrt{\frac{\hat{\alpha_r}\hat{T_0}^4}{\hat{\rho}_0\mathbb{P}}}\,, \tag{22c}$$

$$\hat{v_0} = M\hat{a_0}\,, \tag{22d}$$

$$\hat{v_1} = v_1\hat{a_0}\,, \tag{22e}$$

$$C_v = \frac{\hat{a_0}^2}{\hat{T_0}\gamma\left(\gamma-1\right)}\,, \tag{22f}$$

$$\hat{\sigma_t} = \frac{c}{3\kappa\hat{a_0}}\,, \tag{22g}$$

$$\hat{\sigma_a} = \sigma_a\frac{\hat{a_0}}{c}\,. \tag{22h}$$

We initialize each radiative shock calculation by setting the left half of the spatial domain equal to the far-upstream condition and the right half equal to the downstream condition. At the boundary, we compute the fluxes using our standard Riemann solver, setting the hydrodynamic unknowns in a ghost cell just to the other side of the boundary equal to the far-stream conditions. This adds stability to the evolution of the shock by reinforcing the steady-state solution while allowing propagating waves to exit the domain. Fig. 3 illustrates this concept for the right boundary. Here, we set the left unknown in an exterior ghost cell equal to the far-downstream conditions, $U_{downstream}$, and compute the boundary advection flux, $F_{N+1/2}$, using our Riemann solver.

Figure 3: **Illustration of the advection boundary conditions for the radiative shock calculations.**

Because sharp slopes in LDFEMs can cause negativities in edge values, we monitor for negativities in the fluid temperature. If a negative temperature is detected, we set all the slopes in that cell to zero so that the edge values are equal to the cell-averages. This preserves energy conservation while eliminating non-physical temperatures at cell-edges.

To compute the time steps during the calculation, we use an adaptive time step control scheme based on a user-specified "target temperature change", ΔT_{targ}. Again, for a given time step, the maximum relative change is computed using:

$$\Delta T = 2\max_i \frac{|T_i^{n+1} - T_i^n|}{T_i^{n+1} + T_i^n}\,. \tag{23}$$

However, because we use an IMEX scheme to solve our rad-hydro system, we must also limit the time step according to the Courant limit associated

Table 1: **fluid properties for radiative shock calculations.**

$\hat{\sigma_a}$	3.9071164263502112e+002
$\hat{\sigma_t}$	8.5314410158161809e+002
$\hat{C_v}$	1.2348000000000001e-001

with the hydrodynamic advection terms. We compute this limit by determining the maximum signal velocity associated with the system and define the maximum hydrodynamic time step to be:

$$\Delta t_H = CFL \Delta x S_{max} \,, \tag{24}$$

where S_{max} is the maximum signal velocity, and CFL is the user-defined Courant condition number such that $0 \leq C \leq 1$. We use the following estimate for S_{max} outlined in [8]:

$$S_{max} = \max_{i \in [1,N]} \left\{ |u_i - a_i|, |u_i + a_i| \right\} \,, \tag{25}$$

where N is the number of cells, u_i is the velocity in cell i, and a_i is the speed of sound in cell i. We then compute the time step as follows:

$$\Delta t^{n+1} = \min \left(\frac{\Delta T_{targ}}{\Delta T} \Delta t^n, \xi \Delta t^n, \Delta t_H, t - t_{fin} \right) \,. \tag{26}$$

The second term ensures that the time step doesn't grow too rapidly by imposing a maximum allowed time step change, ξ, and the fourth term forces the final time step to end the calculation at t_{fin}. In order to ensure that the temperature doesn't vary too much, ΔT is also compared with a maximum allowed temperature change, ΔT_{max}. If $\Delta T > \Delta T_{max}$, then the time step $\Delta t^{n+1/2}$ is reduced by a factor of 1/3, and the calculation is repeated from t_n. In our calculations, we set $CFL = 0.3$, $\Delta T_{targ} = 1.01$, $\Delta T_{max} = 1.012$, and $\xi = 1.5$.

5.1. Radiative Shock Solutions

We test our algorithm over a range of the radiative shocks presented in [**?**], which incorporate a variety of structural features. For each of these shocks, we set $\mathbb{P} = 1e-4$, $\gamma = 5/3$, $\kappa = 1$, and $\sigma_a = 1e6$, and the fluid properties are given in Table 1.

First, we compute the Mach 1.2 shock, which has a hydrodynamic shock but no ISP. Table **??** shows the initial conditions; the final time of the calculation is 0.5 shakes. Figs. **??** and **??** compare our results with the semi-analytic solutions for the density and fluid and radiation temperatures, respectively, and again, we see good agreement between the two. In this solution, we see a discontinuity in both the density and fluid temperature due to the hydrodynamic shock, and the maximum temperature is bounded by the far-downstream temperature, since there is no ISP to drive it further.

A Mach 2 radiative shock problem was taken from [**?**]. The material properties are uniform and are given in Table 2. Initial conditions in the pre-shock and post-shock regions are given in Table 3. Figure 4 shows the numerical solution computed with 300 cells and a CFL of 0.6, using the van Leer slope limiter; the comparison to the reference solution shows excellent agreement.

Table 2: Material property values for the Mach 2 radiative shock problem

Parameter	*Value*
σ_a	390.71164263502112
σ_t	853.14410158161809
c_v	0.12348

Table 3: Initial condition values for the Mach 2 radiative shock problem

Parameter	*Pre-shock Value*	*Post-shock Value*
ρ	1	2.2860748989303659
u	0.23426480742954117	0.10247468599526272
E	3.9788000000000004e-2	7.0649692950433357e-2
$\mathcal{E}$	1.3720000000000002e-6	2.5560936967521927e-5
$\mathcal{F}$	0	0

The most structurally complex shock that we compute is the Mach 2 shock, which has both a hydrodynamic shock and an ISP. The initial conditions are given by Table **??**, and the final time of the calculation is 1 shake. Figs. **??** and **??** show our results compared with the semi-analytic solutions. In each of these figures, we can see the effects of the hydrodynamic shock, causing a discontinuity in both the fluid density and temperature. We can also see the Zel'dovich spike, caused by the ISP embedded within the hydrodynamic shock, driving up the fluid temperature at the shock front. This

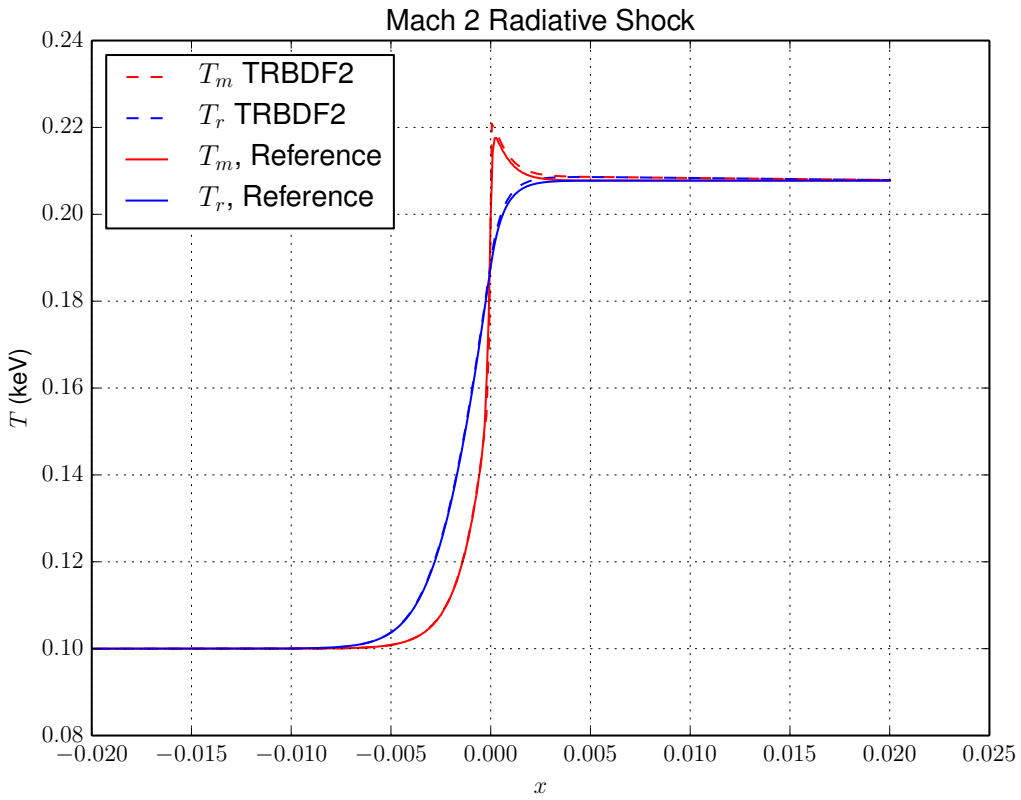

Figure 4: Comparison of Mach 2 radiative shock solution to reference solution

spike leads to the relaxation region downstream as the fluid temperature and radiation temperature equilibrate. Fig. **??** shows the Zel'dovich spike and relaxation region in more detail. Here, we can see that our results still show very good agreement with the semi-analytic solution.

6. Conclusions and Future Work

References

[1] R. G. McClarren, T. M. Evans, R. B. Lowrie, J. D. Densmore, Semi-Implicit Time Integration for Pn Thermal Radiative Transfer, Journal of Computational Physics 196 (2004) 566–590.

[2] R. B. Lowrie, A Comparison of Implicit Time Integration Methods for

Nonlinear Relaxation and Diffusion, Journal of Computational Physics 196 (2004) 566–590.

[3] D. A. Knoll, R. B. Lowrie, J. E. Morel, Numerical Analysis of Time Integration Errors for Nonequilibrium Radiation Diffusion, Journal of Computational Physics 226 (2007) 1332–1347.

[4] G. L. Olson, Second-Order Time Evolution of Pn Equations for Radiation Transport, Journal of Computational Physics 228 (2009) 3027–3083.

[5] T. S. Axelrod, P. F. Dubois, C. E. R. Jr., An Implicit Scheme for Calculating Time- and Fequency-Dependent Flux Limited Radiation Diffusion in One Dimension, Journal of Computational Physics 54 (1984) 205–220.

[6] J. M. Stone, D. Mihalas, Upwind Monotonic Interpolation Methods for the Solution of the Time Dependent Radiative Transfer Equation, Journal of Computational Physics 100 (1992) 402–408.

[7] P. N. Brown, D. E. Shumaker, C. S. Woodward, Fully Implicit Solution of Large-Scale Non-equilibrium Radiation Diffusion with High Order Time Integration, Journal of Computational Physics 204 (2005) 760–783.

[8] E. Toro, Riemann Solvers and Numerical Methods for Fluid Dynamics: A Practical Introduction, Springer, 1999.

[9] R. B. Lowrie, J. E. Morel, J. A. Hittinger, The Coupling of Radiation and Hydrodynamics, Astrophysics Journal 521 (1999) 432–450.

[10] J. W. Bates, D. A. Knoll, W. J. Rider, R. B. Lowrie, V. A. Mousseau, On Consistent Time-Integration Methods for Radiation Hydrodynamics in the Equilibrium Diffusion Limit: Low-Energy-Density Regime, Journal of Computational Physics 167 (2001) 99–130.

[11] W. Dai, P. R. Woodward, Numerical Simulations for Radiation Hydrodynamics. I. Diffusion Limit, Journal of Computational Physics 142 (1998) 182–207.

[12] M. Sekora, J. Stone, A Higher Order Godunov Method for Radiation Hydrodynamics: Radiation Subsystem, Communication in Applied and Computational Mathematics 4 (2009) 135–152.

[13] S. Y. Kadioglu, A Second Order Self-Consistent IMEX Method for Radiation Hydrodynamics, Journal of Computational Physics 229 (2010) 8313–8332.

[14] S. Y. Kadioglu, A Fully Second Order Implicit/Explicit Time Integration Technique for Hydrodynamics Plus Nonlinear Heat Conduction Problems, Journal of Computational Physics 9 (2010) 3237–3249.

[15] R. E. Bank, W. M. Coughran, Jr., W. Fichtner, E. H. Grosse, D. J. Rose, R. K. Smith, Transient Simulation of Silicon Devices and Circuits, IEEE Transactions on Computer-Aided Design of Integrated Circuits and Systems 4 (1985) 436–451.

[16] J. D. Edwards, J. E. Morel, Nonlinear Variants of the TR/BDF2 Method for Thermal Radiative Diffusion, Journal of Computational Physics 230 (2011) 1198–1214.

[17] E. W. Larsen, J. E. Morel, J. W. F. Miller, Asymptotic Solutions of Numerical Transport Problems in Optically Thick, Diffusive Regimes, Journal of Computational Physics 69 (1987) 283–324.

[18] R. B. Lowrie, J. E. Morel, Issues with High-Resolution Godunov Methods for Radiation Hydrodynamics, Journal of Quantitative Spectroscopy & Radiative Transfer 69 (2001) 475–489.

[19] Z. J. Wang, High-order Methods for the Euler and NavierStokes Equations on Unstructured Grids, Progress in Aerospace Science 43 (2007) 1–41.

[20] M. L. Adams, Discontinuous Finite Element Transport Solutions in Thick Diffusive Problems, Nuclear Science and Engineering 137 (2001) 298–333.

[21] R. G. McClarren, R. B. Lowrie, The Effects of Slope Limiting on Asymptotic Preserving Numerical Methods for Hyperbolic Conservation Laws, Journal of Computational Physics 227 (2008) 9711–9726.

Appendix A. Details of the Radiation-Hydrodynamics Method

Here we give a detailed description of our radiation-hydrodynamics method. First, we define some notation; the following are quantities stored throughout the calculation:

Radiation angular intensities	$\mathbf{R}^n \equiv \{\Psi^{\pm}_{i,L}, \Psi^{\pm}_{i,R}\} \quad \forall i$
Conservative hydrodynamics variables	$\mathbf{H}^n \equiv \{\rho^n_i, (\rho u)^n_i, E^n_i\} \quad \forall i$
MHM fluid internal energy slopes	$\delta e^n \equiv \{\delta e^n_i\} \quad \forall i$
MHM conservative variable slopes	$\bar{\Delta}^n \equiv \{\bar{\Delta}\rho^n_i, \bar{\Delta}(\rho u)^n_i, \bar{\Delta}E^n_i\} \quad \forall i$
Macroscopic cross sections	$\sigma^n \equiv \{\sigma^n_{s,i,L}, \sigma^n_{s,i,R}, \sigma^n_{a,i,L}, \sigma^n_{a,i,R}, \sigma^n_{t,i,L}, \sigma^n_{t,i,R}\} \quad \forall i$

Other quantities are computed when needed. The solution for a time step $t^n \to t^{n+1}$ consists of four nonlinear solves:

1. Crank-Nicolson step from t^n to $t^{n+\frac{1}{4}}$ (Cycle 1 Predictor)
2. Crank-Nicolson step from t^n to $t^{n+\frac{1}{2}}$ (Cycle 1 Corrector)
3. Crank-Nicolson step from $t^{n+\frac{1}{2}}$ to $t^{n+\frac{3}{4}}$ (Cycle 2 Predictor)
4. TR/BDF-2 step from $t^{n+\frac{1}{2}}$ to t^{n+1} (Cycle 2 Corrector)

1. **Perform Cycle 1 Predictor.**
   (a) **Perform MUSCL-Hancock Predictor.** First, slopes Δ^n are computed via Equations (B.3) and (B.4), optionally applying a slope limiter. Then a linear-discontinuous representation of the solution is created via Equation (B.6), and the the MUSCL-Hancock predictor is performed to obtain $\mathbf{H}^*$, the homogeneous hydrodyamics solution at $t^{n+\frac{1}{4}}$, via Equation (B.7).
   (b) **Perform nonlinear iterations.** Iteration of the $t^{n+\frac{1}{4}}$ solution is required since the system of equations is nonlinear.
      i. **Update velocities.** The Crank-Nicolson discretization of the velocity update equation, Equation (B.9), is solved to obtain new velocities at cell centers, $\{u^{k+1}_i\}$. Evaluation of the radiation quantities $\mathcal{E}$ and $\mathcal{F}$ at cell centers is achieved by averaging the left and right values.
      ii. **Update radiation.** The Crank-Nicolson discretization of the S-2 equations, Equations (B.27) and (B.28) are solved, employing the linearization given in Section Appendix B.6. Evaluation of the densities and velocities at the edges is achieved

using using the cell-centered values in conjunction with the slopes Δ^n. Evaluation of the material energy E at edges is achieved using the internal energy slopes δe^n from a previous radiation solve. The computation of this slope is described in Section Appendix B.4.

iii. **Update internal energies.** The internal energies are updated in accordance with the linearization procedure given is Section Appendix B.6. The update equations produce edge values $\{e_{i,L}^{k+1}, e_{i,R}^{k+1}\}$. These left and right values are added to the kinetic energy at edges to produce cell-averaged values for the total energy $\{E_i^{k+1}\}$, which are used in the subsequent iteration. The values of δe are stored for the next radiation solve. Cross sections that are updated if they are functions of the hydrodynamic state of the fluid.

iv. **Check convergence.** The new solutions $\mathbf{R}^{k+1}$ and $\mathbf{H}^{k+1}$ are compared with the previous iteration solutions $\mathbf{R}^k$ and $\mathbf{H}^k$ to determine if convergence has been achieved. If the solutions have not converged, then the computation returns to Step 1(b)i.

2. **Perform Cycle 1 Corrector.** This step proceeds just as the predictor step, except that the MUSCL-Hancock corrector step given by Equation (B.8) is used instead of the MUSCL-Hancock predictor step, and the step goes from t^n to $t^{n+\frac{1}{2}}$ instead of t^n to $t^{n+\frac{1}{4}}$. No new hydrodynamic slopes are computed; evaluation of edge densities and velocities use Δ^n. However, evaluation of edge internal energies in the nonlinear iteration use $\delta e^{n+1/4}$ (CURRENTLY WE JUST USE δe^n, NEED TO CHECK THIS). At the end of the cycle, the new internal energy slopes $\delta e^{n+\frac{1}{2}}$ are saved for the next cycle.
3. **Perform Cycle 2 Predictor.** This step proceeds just as the Cycle 1 predictor step, except that the step goes from $t^{n+\frac{1}{2}}$ to $t^{n+\frac{3}{4}}$ instead of t^n to $t^{n+\frac{1}{4}}$. As in Cycle 1, new slopes are computed in the MUSCL-Hancock predictor step; these slopes $\Delta^{n+\frac{1}{2}}$ are then used for evaluation of edge densities and velocities in the remainder of the cycle. Evaluation of edge internal energies and temperatures use the internal energies saved from the end of Cycle 1, $\delta e^{n+\frac{1}{2}}$.
4. **Perform Cycle 2 Corrector.** This step proceeds as the Cycle 1 corrector step, except that the time step goes from $t^{n+\frac{1}{2}}$ to t^{n+1}, and the time discretization of the equations is a form of TR/BDF-2 instead of

Crank-Nicolson, so values at t^n are used in the temporal discretization. Slopes $\Delta^{n+\frac{1}{2}}$ and $\delta e^{n+\frac{3}{4}}$ (CURRENTLY WE JUST USE $\delta e^{n+\frac{1}{2}}$, NEED TO CHECK THIS) are again used to evaluate edge quantities. At the end of the cycle, the new internal energy slopes δe^{n+1} are saved for the next cycle.

5. **Store values for next time step.** At this point, the old solutions, hydrodynamics slopes, internal energy slopes, and cross sections are saved for the next time step.

Appendix B. The Discretized Equations

Appendix B.1. MUSCL-Hancock Equations

The homogeneous Euler equations may be expressed in conservative form as

$$\frac{\partial \mathbf{H}}{\partial t} + \nabla \cdot \mathbf{F}(\mathbf{H}) = \mathbf{0}\,, \tag{B.1}$$

where $\mathbf{H}$ is a vector of the conservative unknowns and $\mathbf{F}(\mathbf{H})$ is the flux associated with each:

$$\mathbf{H} = \begin{bmatrix} \rho \\ \rho u \\ E \end{bmatrix}\,, \qquad \mathbf{F}(\mathbf{H}) = \begin{bmatrix} \rho u \\ \rho u^2 + p \\ (E+p)u \end{bmatrix}\,. \tag{B.2}$$

The first half of a MUSCL-Hancock step $t^n \to t^n + \Delta t$ starts by constructing a linear representation of the solution using slopes Δ_i^n:

$$\Delta_i^n = \frac{1}{2}\Delta\mathbf{H}^n_{i-\frac{1}{2}} + \frac{1}{2}\Delta\mathbf{H}^n_{i+\frac{1}{2}}\,, \tag{B.3}$$

$$\Delta\mathbf{H}^n_{i-\frac{1}{2}} = \mathbf{H}^n_i - \mathbf{H}^n_{i-1}\,, \quad \Delta\mathbf{H}^n_{i+\frac{1}{2}} = \mathbf{H}^n_{i+1} - \mathbf{H}^n_i\,, \tag{B.4}$$

These slopes are optionally limited via slope limiters ξ_i:

$$\bar{\Delta}_i = \xi_i \Delta_i\,. \tag{B.5}$$

We have chosen to use the double-minmod slope limiter [**?**]. If no slope limiter is used, then $\xi_i = 1$. The linear representation of the solution is built as

$$\mathbf{H}^n_{i,L} = \mathbf{H}^n_i - \frac{\bar{\Delta}^n_i}{2}\,, \quad \mathbf{H}^n_{i,R} = \mathbf{H}^n_i + \frac{\bar{\Delta}^n_i}{2}\,, \tag{B.6}$$

This representation is then evolved by half a time step:

$$\mathbf{H}_i^{n+\frac{1}{2}} = \mathbf{H}_i^n - \frac{\frac{1}{2}\Delta t}{\Delta x}\left(\mathbf{F}(\mathbf{H}_{i,R}^n) - \mathbf{F}(\mathbf{H}_{i,L}^n)\right) . \tag{B.7}$$

The second half of a MUSCL-Hancock step employs a Riemann solver to compute the fluxes at time $n + \frac{1}{2}$:

$$\mathbf{H}_i^{n+1} = \mathbf{H}_i^n - \frac{\Delta t}{\Delta x}\left(\mathbf{F}_{i+\frac{1}{2}}^{n+\frac{1}{2}} - \mathbf{F}_{i-\frac{1}{2}}^{n+\frac{1}{2}}\right) . \tag{B.8}$$

Appendix B.2. Fluid Momentum Source Update Equation

The Crank-Nicolson discretization of the velocity update equation is the following:

$$\frac{\rho_i^*\left(u_i^{k+1} - u_i^*\right)}{\Delta t} = \frac{1}{2}\left[\frac{\sigma_t}{c}\left(\mathcal{F} - \frac{4}{3}\mathcal{E}u\right)\right]_i^n + \frac{1}{2}\left[\frac{\sigma_t}{c}\left(\mathcal{F} - \frac{4}{3}\mathcal{E}u\right)\right]_i^k . \tag{B.9}$$

The BDF2 discretization of the velocity update equation is the following:

$$\begin{aligned}\frac{\rho_i^*\left(u_i^{k+1} - u_i^*\right)}{\Delta t} =& \frac{1}{6}\left[\frac{\sigma_t}{c}\left(\mathcal{F} - \frac{4}{3}\mathcal{E}u\right)\right]_i^{n-1} + \frac{1}{6}\left[\frac{\sigma_t}{c}\left(\mathcal{F} - \frac{4}{3}\mathcal{E}u\right)\right]_i^n \\ &+ \frac{2}{3}\left[\frac{\sigma_t}{c}\left(\mathcal{F} - \frac{4}{3}\mathcal{E}u\right)\right]_i^k .\end{aligned} \tag{B.10}$$

The momentum source terms in these equations are computed by taking the linear average of the momentum source expressions evaluated at the edges, e.g.,

$$\begin{aligned}\left[\frac{\sigma_t}{c}\left(\mathcal{F} - \frac{4}{3}\mathcal{E}u\right)\right]_i =& \frac{1}{2}\left[\frac{\sigma_{t,i,L}}{c}\left(\mathcal{F}_{i,L} - \frac{4}{3}\mathcal{E}_{i,L}u_{i,L}\right)\right] \\ &+ \frac{1}{2}\left[\frac{\sigma_{t,i,R}}{c}\left(\mathcal{F}_{i,R} - \frac{4}{3}\mathcal{E}_{i,R}u_{i,R}\right)\right] .\end{aligned} \tag{B.11}$$

Appendix B.3. Fluid Energy Source Update Equation

The energy source update equations are evaluated at the edges and thus hydrodynamic quantities need to be evaluated at the edges. The stored solution values consist of the cell average unknowns for the conservative variables

$[\rho, \rho u, E]$ and their slopes Δ, which come from the predictor step of MUSCL-Hancock, as given by Equation (B.3). Evaluation of edge densities is achieved by applying the slopes as given by Equation (B.6):

$$\rho_{i,L}^k = \rho_i^k - \frac{\Delta\rho_i^n}{2}\,. \tag{B.12}$$

Note that the slopes Δ are only updated in the MUSCL-Hancock predictor step. Thus, quantities at t^{n+1} also use the Δ^n slopes. For the BDF2 discretization, where evaluation of quantities at t^{n-1} is required, the old slopes Δ^{n-1} are used. Evaluation of edge velocities is achieved by evaluating the edge conservative variables ρ and ρu and then computing velocity from these, e.g.,

$$u_{i,L}^k = \frac{(\rho u)_{i,L}^k}{\rho_{i,L}^k} = \frac{(\rho u)_i^k - \frac{\Delta(\rho u)_i^n}{2}}{\rho_i^k - \frac{\Delta\rho_i^n}{2}}\,. \tag{B.13}$$

As explained in Section Appendix B.4, internal energy unknowns, and thus material temperature, use slopes that are independent of the MUSCL-Hancock slopes. These internal energy slopes are denoted by δe. Evaluation of edge internal energies is thus performed as follows:

$$e_{i,L}^k = e_i^k - \frac{\delta e_i^n}{2}\,. \tag{B.14}$$

Edge temperatures are computed from the edge internal energies:

$$T_{i,L}^k = \frac{e_{i,L}^k}{c_v}\,. \tag{B.15}$$

Again, quantities at t^{n+1} still use old slopes δe^n. These slopes are updated at the end of each full MUSCL-Hancock step, i.e., when the nonlinear iteration for the corrector step converges, the slopes δe_i^{n+1} are computed from the converged edge internal energies:

$$\delta e_i^{n+1} = e_{i,R}^{k+1} - e_{i,L}^{k+1}\,. \tag{B.16}$$

The Crank-Nicolson discretization of the energy update equation is

$$\begin{aligned}\frac{E_{i,L}^{k+1} - E_{i,L}^*}{\Delta t} = &-\frac{1}{2}\left[\sigma_a c\left(aT^4 - \mathcal{E}\right)\right]_{i,L}^n - \frac{1}{2}\sigma_{a,i,L}^k c\left[aT^4 - \mathcal{E}\right]_{i,L}^{k+1} \\ &+ \frac{1}{2}\left[\sigma_t \frac{u}{c}\left(\mathcal{F} - \frac{4}{3}\mathcal{E}u\right)\right]_{i,L}^n + \frac{1}{2}\left[\sigma_t \frac{u}{c}\left(\mathcal{F} - \frac{4}{3}\mathcal{E}u\right)\right]_{i,L}^k\,.\end{aligned} \tag{B.17}$$

The right edge equations are identical in form, obtained by replacing "L" with "R" in the left edge equations. The BDF2 discretization of the energy update equation is

$$\begin{aligned}\frac{E_{i,L}^{k+1} - E_{i,L}^{*}}{\Delta t} = &- \frac{1}{6}\left[\sigma_a c\left(aT^4 - \mathcal{E}\right)\right]_{i,L}^{n-1} - \frac{1}{6}\left[\sigma_a c\left(aT^4 - \mathcal{E}\right)\right]_{i,L}^{n} \\ &- \frac{2}{3}\sigma_{a,i,L}^{k} c\left[aT^4 - \mathcal{E}\right]_{i,L}^{k+1} + \frac{1}{6}\left[\sigma_t \frac{u}{c}\left(\mathcal{F} - \frac{4}{3}\mathcal{E}u\right)\right]_{i,L}^{n-1} \\ &+ \frac{1}{6}\left[\sigma_t \frac{u}{c}\left(\mathcal{F} - \frac{4}{3}\mathcal{E}u\right)\right]_{i,L}^{n} + \frac{2}{3}\left[\sigma_t \frac{u}{c}\left(\mathcal{F} - \frac{4}{3}\mathcal{E}u\right)\right]_{i,L}^{k}.\end{aligned} \tag{B.18}$$

The energy update to the Note that these energy update equations are not in the form in which they are actually solved in practice; the implicit term $\sigma_a^k ac(T^{k+1})^4$ must be linearized. This procedure is detailed in Section Appendix B.6. The final form of the energy update equation is a direct update to the edge internal energies $\{e_{i,L}^{k+1}, e_{i,R}^{k+1}\}$.

Appendix B.4. Using Radiation Internal Energy Slopes

As discussed in the introduction, the radiation solver and hydro solver use different internal energy slopes as an approach to preserve the equilibrium diffusion limit. The implementation of separate slopes is a proof of concept for higher dimensions. To mitigate confusion, in this section we will denote the hydro-state internal energy variables as e and the internal energy variables coming from the non-linear radiation solves as e^r. Care must be taken to ensure that total energy is conserved. The modified slopes are only applied to the implicit terms in each nonlinear solve.

During the MHM solve, we use the standard slope reconstruction formulas to advect variables to state U^* (or U^{**}), including total energy E. Then, in the non-linear iteration loop for the radiation and internal energy densities we use a modified slope for E^*, denoted ΔE^{r*}, that will preserve the diffusion limit. This ΔE^{r*} is based on the edge values of e^r of *the last iteration of the previous nonlinear radiation solve*. For example, if we are solving the cycle 1 corrector from state e^* to $e^{n+1/2}$, we use the edge values of e^r from the last iteration of the solve for $e^{r,n+1/4}$ to construct the slopes for $\Delta E^{r,*}$. The value of $\Delta E^{r,*}$ does not change over the duration of the nonlinear solve.

For the nonlinear solve we need the to use δe^r to construct ΔE^{*r} in the next solve (and thus the values $E_{R/L}^* = E_i^* \pm \frac{1}{2}\Delta E^{r*}$ needed for the LD

radiation solve). We approximate this slope based on the hydro values for E^* as:

$$\Delta E^{r*} = E_R^{r*} - E_L^{r*} \tag{B.19}$$

where

$$E_R^{r*} = \rho_R^* \left((u_R^*)^2 + e_i^* + \delta e^{r,n+1/4} \right), \tag{B.20}$$

$$E_L^{r*} = \rho_R^* \left((u_L^*)^2 + e_i^* - \delta e^{r,n+1/4} \right), \tag{B.21}$$

and subscript i denotes cell average quantities. The edge values of ρ and u are evaluated using the MHM slopes as usual. Once we have completed the nonlinear solve for $e_{L/R}^{r,n+1/2}$, we must compute the change made to the cell-averaged total energy for the next MHM solve, such that total energy is conserved. The formula for the new total energy is

$$E_i^{n+1/2} = \frac{1}{2} \left[\rho_L \left(\frac{1}{2} u_L^2 + e_L^r \right) + \rho_R \left(\frac{1}{2} u_R^2 + e_R^r \right) \right]^{n+1/2} \tag{B.22}$$

where all variables are at time $t^{n+1/2}$. The internal energy slopes are computed and stored for the next nonlinear solve. For the first solve, the internal energy slopes are assumed zero.

Appendix B.5. S_2 Equations

A lumped linear discontinuous (LLD) spatial discretization is employed for the S_2 equations, so the angular flux unknowns are the left and right values $\Psi_{i,L}^{\pm}$ and $\Psi_{i,R}^{\pm}$ for each cell i. The spatially discretized equations result from integrating each half cell $(x_i - \frac{h_i}{2}, x_i)$ and $(x_i, x_i + \frac{h_i}{2})$, where x_i is the cell center, h_i is the cell width, and the cell average and edge fluxes are defined as

$$\Psi_i^{\pm} = \frac{1}{2} \left(\Psi_{i,L}^{\pm} + \Psi_{i,R}^{\pm} \right), \tag{B.23}$$

$$\Psi_{i+\frac{1}{2}}^{+} = \Psi_{i,R}^{+}, \qquad \Psi_{i+\frac{1}{2}}^{-} = \Psi_{i+1,L}^{-}. \tag{B.24}$$

Appendix B.5.1. Steady-State

Using an LLD discretization, the steady-state S_2 equations, obtained by dropping the $\frac{\partial \Psi^{\pm}}{\partial t}$ term in Equation (**??**), become

$$\frac{2\mu^{\pm}}{h_i} \left(\Psi_i^{\pm,k+1} - \Psi_{i-\frac{1}{2}}^{\pm,k+1} \right) + \sigma_{t,i,L}^k \Psi_{i,L}^{\pm,k+1} - \frac{\sigma_{s,i,L}^k}{2} \phi_{i,L}^{k+1} = \mathcal{Q}_{i,L}^{\pm,k}, \tag{B.25}$$

$$\frac{2\mu^{\pm}}{h_i} \left(\Psi_{i+\frac{1}{2}}^{\pm,k+1} - \Psi_i^{\pm,k+1} \right) + \sigma_{t,i,R}^k \Psi_{i,R}^{\pm,k+1} - \frac{\sigma_{s,i,R}^k}{2} \phi_{i,R}^{k+1} = \mathcal{Q}_{i,R}^{\pm,k}. \tag{B.26}$$

Appendix B.5.2. Crank-Nicolson

$$\begin{aligned}\frac{1}{c}\frac{\Psi_{i,L}^{\pm,k+1}-\Psi_{i,L}^{\pm,n}}{\Delta t} =& -\frac{1}{2}\frac{2\mu^{\pm}}{h_i}\left(\Psi_{i}^{\pm,n}-\Psi_{i-\frac{1}{2}}^{\pm,n}\right)-\frac{1}{2}\frac{2\mu^{\pm}}{h_i}\left(\Psi_{i}^{\pm,k+1}-\Psi_{i-\frac{1}{2}}^{\pm,k+1}\right)\\ &-\frac{1}{2}\sigma_{t,i,L}^{n}\Psi_{i,L}^{\pm,n}-\frac{1}{2}\sigma_{t,i,L}^{k}\Psi_{i,L}^{\pm,k+1}\\ &+\frac{1}{2}\frac{\sigma_{s,i,L}^{n}}{2}\phi_{i,L}^{n}+\frac{1}{2}\frac{\sigma_{s,i,L}^{k}}{2}\phi_{i,L}^{k+1}\\ &+\frac{1}{2}\mathcal{Q}_{i,L}^{\pm,n}+\frac{1}{2}\mathcal{Q}_{i,L}^{\pm,k}\,.\end{aligned} \tag{B.27}$$

$$\begin{aligned}\frac{1}{c}\frac{\Psi_{i,R}^{\pm,k+1}-\Psi_{i,R}^{\pm,n}}{\Delta t} =& -\frac{1}{2}\frac{2\mu^{\pm}}{h_i}\left(\Psi_{i+\frac{1}{2}}^{\pm,n}-\Psi_{i}^{\pm,n}\right)-\frac{1}{2}\frac{2\mu^{\pm}}{h_i}\left(\Psi_{i+\frac{1}{2}}^{\pm,k+1}-\Psi_{i}^{\pm,k+1}\right)\\ &-\frac{1}{2}\sigma_{t,i,R}^{n}\Psi_{i,R}^{\pm,n}-\frac{1}{2}\sigma_{t,i,R}^{k}\Psi_{i,R}^{\pm,k+1}\\ &+\frac{1}{2}\frac{\sigma_{s,i,R}^{n}}{2}\phi_{i,R}^{n}+\frac{1}{2}\frac{\sigma_{s,i,R}^{k}}{2}\phi_{i,R}^{k+1}\\ &+\frac{1}{2}\mathcal{Q}_{i,R}^{\pm,n}+\frac{1}{2}\mathcal{Q}_{i,R}^{\pm,k}\,.\end{aligned} \tag{B.28}$$

Appendix B.5.3. TR/BDF-2

$$\begin{aligned}\frac{1}{c}\frac{\Psi_{i,L}^{\pm,k+1}-\Psi_{i,L}^{\pm,n}}{\Delta t} =& -\frac{1}{6}\frac{2\mu^{\pm}}{h_i}\left(\Psi_{i}^{\pm,n-1}-\Psi_{i-\frac{1}{2}}^{\pm,n-1}\right)-\frac{1}{6}\frac{2\mu^{\pm}}{h_i}\left(\Psi_{i}^{\pm,n}-\Psi_{i-\frac{1}{2}}^{\pm,n}\right)\\ &-\frac{2}{3}\frac{2\mu^{\pm}}{h_i}\left(\Psi_{i}^{\pm,k+1}-\Psi_{i-\frac{1}{2}}^{\pm,k+1}\right)\\ &-\frac{1}{6}\sigma_{t,i,L}^{n-1}\Psi_{i,L}^{\pm,n-1}-\frac{1}{6}\sigma_{t,i,L}^{n}\Psi_{i,L}^{\pm,n}-\frac{2}{3}\sigma_{t,i,L}^{k}\Psi_{i,L}^{\pm,k+1}\\ &+\frac{1}{6}\frac{\sigma_{s,i,L}^{n-1}}{2}\phi_{i,L}^{n-1}+\frac{1}{6}\frac{\sigma_{s,i,L}^{n}}{2}\phi_{i,L}^{n}+\frac{2}{3}\frac{\sigma_{s,i,L}^{k}}{2}\phi_{i,L}^{k+1}\\ &+\frac{1}{6}\mathcal{Q}_{i,L}^{\pm,n-1}+\frac{1}{6}\mathcal{Q}_{i,L}^{\pm,n}+\frac{2}{3}\mathcal{Q}_{i,L}^{\pm,k}\,,\end{aligned} \tag{B.29}$$

$$\begin{aligned}\frac{1}{c}\frac{\Psi_{i,R}^{\pm,k+1}-\Psi_{i,R}^{\pm,n}}{\Delta t} =& -\frac{1}{6}\frac{2\mu^{\pm}}{h_i}\left(\Psi_{i+\frac{1}{2}}^{\pm,n-1}-\Psi_{i}^{\pm,n-1}\right)-\frac{1}{6}\frac{2\mu^{\pm}}{h_i}\left(\Psi_{i+\frac{1}{2}}^{\pm,n}-\Psi_{i}^{\pm,n}\right)\\ &-\frac{2}{3}\frac{2\mu^{\pm}}{h_i}\left(\Psi_{i+\frac{1}{2}}^{\pm,k+1}-\Psi_{i}^{\pm,k+1}\right)\\ &-\frac{1}{6}\sigma_{t,i,R}^{n-1}\Psi_{i,R}^{\pm,n-1}-\frac{1}{6}\sigma_{t,i,R}^{n}\Psi_{i,R}^{\pm,n}-\frac{2}{3}\sigma_{t,i,R}^{k}\Psi_{i,R}^{\pm,k+1}\\ &+\frac{1}{6}\frac{\sigma_{s,i,R}^{n-1}}{2}\phi_{i,R}^{n-1}+\frac{1}{6}\frac{\sigma_{s,i,R}^{n}}{2}\phi_{i,R}^{n}+\frac{2}{3}\frac{\sigma_{s,i,R}^{k}}{2}\phi_{i,R}^{k+1}\\ &+\frac{1}{6}\mathcal{Q}_{i,R}^{\pm,n-1}+\frac{1}{6}\mathcal{Q}_{i,R}^{\pm,n}+\frac{2}{3}\mathcal{Q}_{i,R}^{\pm,k}\,,\end{aligned} \tag{B.30}$$

Appendix B.6. Linearization of Equations for General Temporal Discretization

Within each solution time step, first the hydro variables are advected (either using local predicted fluxes or a Riemann solver). Then, a non-linear system must be solved iteratively with iteration index k. Consider the case of a non-linear system over a single step from t_n to t_{n+1}. We will combine all known source terms as Q_k, which are known from previous states in time or the previous iteration k. To linearize the system, we perform the standard approach of linearizing the Planckian function about some temperature near T^{n+1}, denoted T^k. For the initial iteration, $T^k = T^n$.

First, the original equation is rewritten as

$$\frac{E^{k+1}-E^{*}}{\Delta t} = -\alpha\left[\sigma_a^k c\left(a(T^{k+1})^4-\mathcal{E}^{k+1}\right)\right]+Q_E^k$$

where for BDF2,

$$\begin{aligned}Q_E^k =& -\frac{1}{6}\left[\sigma_a c\left(aT^4-\mathcal{E}\right)\right]^{n-1}-\frac{1}{6}\left[\sigma_a c\left(aT^4-\mathcal{E}\right)\right]^{n}\\ &+\frac{1}{6}\left[\sigma_t\frac{u}{c}\left(\mathcal{F}-\frac{4}{3}\mathcal{E}u\right)\right]^{n-1}+\frac{1}{6}\left[\sigma_t\frac{u}{c}\left(\mathcal{F}-\frac{4}{3}\mathcal{E}u\right)\right]^{n}+\frac{2}{3}\left[\sigma_t\frac{u}{c}\left(\mathcal{F}-\frac{4}{3}\mathcal{E}u\right)\right]^{k},\end{aligned} \tag{B.31}$$

for CN,

$$Q_E^k = -\frac{1}{2}\left[\sigma_a c\left(aT^4 - \mathcal{E}\right)\right]^n + \frac{1}{2}\left[\sigma_t \frac{u}{c}\left(\mathcal{F} - \frac{4}{3}\mathcal{E}u\right)\right]^n + \frac{1}{2}\left[\sigma_t \frac{u}{c}\left(\mathcal{F} - \frac{4}{3}\mathcal{E}u\right)\right]^k, \quad \text{(B.32)}$$

and for BE,

$$Q_E^k = \sigma_t \frac{u}{c}\left(\mathcal{F} - \frac{4}{3}\mathcal{E}u\right)^k.$$

The scale factor α for BE, CN, and BDF2 is 1, $\frac{1}{2}$, and $\frac{2}{3}$, respectively. With these definitions, the Planckian source term becomes

$$\sigma_a^k ac\left(T^{k+1}\right)^4 = \left(1-\nu_\alpha^k\right)\sigma_a^k ac(T^k)^4 + \sigma_a^k c\nu_\alpha^k \mathcal{E}^{k+1} + \frac{\nu_\alpha^k}{\alpha}Q_E^k - \frac{\rho\nu_\alpha^k}{\alpha\Delta t}\left[(e^k - e^*) + \frac{1}{2}((u^{k+1})^2 - (u^*)^2)\right]. \quad \text{(B.33)}$$

with

$$\nu_\alpha^k = \frac{\alpha\sigma_a c\Delta t\frac{\beta^k}{\rho}}{1+\alpha\sigma_a c\Delta t\frac{\beta^k}{\rho}}. \quad \text{(B.34)}$$

and $\beta^k = \frac{4a(T^k)^3}{c_v^k}$. The energy update equation becomes

$$e^{k+1} = \alpha\frac{(1-\nu_\alpha)\Delta t}{\rho}\left[\sigma_a^k c\left(\mathcal{E}^{k+1} - a(T^k)^4\right) + \frac{Q_E^k}{\alpha}\right] - (1-\nu_\alpha)\left(\frac{1}{2}[(u^{k+1})^2 - (u^*)^2]\right) + (1-\nu_\alpha)e^* + \nu_\alpha e^k. \quad \text{(B.35)}$$

After solving for $\mathcal{E}^{k+1}$, a new internal energy can be estimated using Eq. (B.35) to conserve energy. Momentum is only conserved to the tolerance of the velocity iterations. Iterations are repeated until convergence, beginning with a solve of Eq. (**??**) with updated radiation quantities. Once the system is converged, the EOS can be used to update p^{n+1}.

Appendix C. Conservation

In the homogeneous hydrodynamics case (where there is no coupling to radiation), one can arrive at a conservation statement for a time step for each

conserved quantity H by summing the MUSCL-Hancock update equation, Equation (B.8), multiplied by cell volume h_i, for all elements:

$$\sum_i h_i H_i^* = \sum_i h_i H_i^n + \Delta t^n \left(F_{\frac{1}{2}}^{H,n+\frac{1}{2}} - F_{N+\frac{1}{2}}^{H,n+\frac{1}{2}} \right) . \tag{C.1}$$

The conservation statement for the momentum source update, obtained for Crank-Nicolson by summing Equation (B.9) multiplied by cell volume h_i for all elements, is

$$\sum_i h_i \rho_i^* u_i^{k+1} = \sum_i h_i (\rho u)_i^* + \Delta t^n \left(\frac{1}{2} \sum_i h_i \frac{\sigma_{t,i}^n}{c} \mathcal{F}_{0,i}^n + \frac{1}{2} \sum_i h_i \frac{\sigma_{t,i}^n}{c} \mathcal{F}_{0,i}^k \right) . \tag{C.2}$$

The conservation statement for the radiation momentum is obtained by manipulating the discretized S-2 equations:

$$\begin{aligned} \sum_i h_i \frac{\mathcal{F}_i^{k+1}}{c^2} = \sum_i h_i \frac{\mathcal{F}_i^n}{c^2} + \Delta t^n \Bigg(& \frac{1}{2}\frac{1}{3c} \left(\Psi_{inc}^{+,n} - \Psi_{inc}^{-,n} + \Psi_{1,L}^{-,n} - \Psi_{N,R}^{+,n} \right) \\ & + \frac{1}{2}\frac{1}{3c} \left(\Psi_{inc}^{+,k+1} - \Psi_{inc}^{-,k+1} + \Psi_{1,L}^{-,k+1} - \Psi_{N,R}^{+,k+1} \right) \\ & - \frac{1}{2} \sum_i h_i \left(\frac{1}{2} \frac{\sigma_{t,i,L}^n}{c} \mathcal{F}_{0,i,L}^n + \frac{1}{2} \frac{\sigma_{t,i,R}^n}{c} \mathcal{F}_{0,i,R}^n \right) \\ & - \frac{1}{2} \sum_i h_i \left(\frac{1}{2} \frac{\sigma_{t,i,L}^k}{c} \mathcal{F}_{0,i,L}^{k+1} + \frac{1}{2} \frac{\sigma_{t,i,R}^k}{c} \mathcal{F}_{0,i,R}^{k+1} \right) \Bigg) . \end{aligned} \tag{C.3}$$

Combining this with the hydrodynamics momentum conservation statement gives the total momentum conservation statement for Crank-Nicolson:

$$\begin{aligned} \sum_i h_i \left(\rho_i^* u_i^{k+1} + \frac{\mathcal{F}_i^{k+1}}{c^2} \right) = \sum_i h_i \left(\rho_i^* u_i^n + \frac{\mathcal{F}_i^n}{c^2} \right) \\ + \Delta t^n \Bigg(F_{\frac{1}{2}}^{n+\frac{1}{2}} - F_{N+\frac{1}{2}}^{n+\frac{1}{2}} + \frac{1}{2}\frac{1}{3c} \left(\Psi_{inc}^{+,n} - \Psi_{inc}^{-,n} + \Psi_{1,L}^{-,n} - \Psi_{N,R}^{+,n} \right) \\ + \frac{1}{2}\frac{1}{3c} \left(\Psi_{inc}^{+,k+1} - \Psi_{inc}^{-,k+1} + \Psi_{1,L}^{-,k+1} - \Psi_{N,R}^{+,k+1} \right) \Bigg) . \end{aligned} \tag{C.4}$$

It is noted that if one is interested in checking the radiation momentum balance for a problem with no fluid motion (thermal radiative transfer only),

then there is the extra momentum deposition terms that do not cancel out in the S_2 equations that must be accounted for. To include MMS sources, the hydro sources can be added directly. The radiation sources must also be included in the momentum. The moments of the extra source are taken in the same way as they are for arriving at the radiation balance equation, resulting in an extra term of $\frac{1}{2c}[\mu^+(Q_L^+ + Q_R^+) - \mu^-(Q_L^- + Q_R^-)]$ to be added to the balance.